Available online at www.sciencedirect.com
SCIENCE DIRECT®
Journal of Sound and Vibration 269 (2004) 669–687
JOURNAL OF SOUND AND VIBRATION
www.elsevier.com/locate/jsvi

# Limit cycle oscillation of missile control fin with structural non-linearity

J.S. Bae, I. Lee*

*Department of Aerospace Engineering, Korea Advanced Institute of Science and Technology (KAIST), 373-1 Gusong-dong, Yusong-gu, Daejon 305-701, South Korea*

Received 2 July 2002; accepted 20 January 2003

**Abstract**

Non-linear aeroelastic characteristics of a deployable missile control fin with structural non-linearity are investigated. A deployable missile control fin is modelled as a two-dimensional typical section model. Doublet-point method is used for the calculation of supersonic unsteady aerodynamic forces, and aerodynamic forces are approximated by using the minimum-state approximation. For non-linear flutter analysis structural non-linearity is represented by an asymmetric bilinear spring and is linearized by using the describing function method. The linear and non-linear flutter analyses indicate that the flutter characteristics are significantly dependent on the frequency ratio. From the non-linear flutter analysis, various types of limit cycle oscillations are observed in a wide range of air speeds below or above the linear divergent flutter boundary. The non-linear flutter characteristics and the non-linear aeroelastic responses are investigated.


## 1. Introduction

Aeroelastic phenomena such as flutter are dynamic instabilities which involve inertia, aerodynamic, and elastic forces of flight vehicles. If an aeroelastic problem occurs in flight, flight vehicle structures may fail. Therefore, it is important to predict aeroelastic characteristics accurately to prevent aeroelastic instabilities.

Under the assumption of structural linearity, aeroelastic analyses of flight vehicles can be easily performed. However, the aeroelastic results under this assumption may not agree well with the physical phenomena because most real structures may have structural non-linearities such as

*Corresponding author. Fax: +82-42-869-3710.
*E-mail addresses:* bjs@asdl.kaist.ac.kr (J.S. Bae), inlee@asdl.kaist.ac.kr (I. Lee).

0022-460X/03/$ - see front matter 
doi:10.1016/S0022-460X(03)00125-1

freeplay, bilinear non-linearity, friction, and hysteresis. Non-linear aeroelastic characteristics are quite different from linear characteristics. Non-linear aeroelastic responses typically include flutter, divergence, limit cycle oscillation (LCO) and chaotic motion.

LCO is a periodic oscillation consisting of a limited number of periods, and chaotic motion is a non-periodic oscillation. When a linear system becomes unstable, the amplitude of the response increases exponentially, whereas a non-linear system has a bounded motion such as LCO or chaotic motion, which may occur below the linear flutter speed. LCO and chaotic motion do not cause the abrupt failure of a structure. However, these motions can cause a structure to be damaged by fatigue and can considerably affect the control systems of flight vehicles. Thus, the effects of structural non-linearities on the aeroelastic characteristics of flight vehicles should be considered in the design stage.

Several investigators have performed non-linear aeroelastic analyses of flight vehicles with structural non-linearities. Woolston et al. [1] analyzed a non-linear aeroelastic system with freeplay, hysteresis, and cubic non-linearity and showed that LCO may occur below the linear flutter boundary. Laurenson and Trn [2] studied flutter of a missile control surface with freeplay using the describing function method. Lee [3] developed an iterative scheme for multiple non-linearities using the describing function method and the structural dynamics modification method. Lee and Tron [4] studied the non-linear aeroelastic characteristics of a CF-18 aircraft with freeplay and bilinear non-linearities in the leading-edge flap hinge and the wing-fold hinge using the describing function method. Yang and Zhao [5] studied the LCO of a typical section model with pitch non-linearity subject to incompressible flow using the Theodorsen function. Lee and Kim [6] studied the LCO and chaotic motion of a missile control surface with freeplay using time-domain analysis. Conner et al. [7] and Tang et al. [8] studied the non-linear aeroelastic characteristics of a typical section with control surface freeplay both numerically and experimentally. Virgin et al. [9] studied the chaotic motion of a typical section and Tang et al. [10] studied the non-linear responses of an airfoil excited by a gust load. Recently, Sheta et al. [11] conducted computational and experimental investigations of a non-linear aeroelastic system with a fifth order polynomial spring.

The purpose of the present study is to investigate the non-linear aeroelastic characteristics of a deployable missile control fin with structural non-linearity. For the simplicity of analysis, the fin is modelled as a two-dimensional typical section. Doublet-point method (DPM) [12] is used for the computation of supersonic unsteady aerodynamic forces, and the method of Karpel [13] is used to approximate the frequency-domain aerodynamic forces. Structural non-linearity is represented by an asymmetric bilinear plunge spring and is linearized using the describing function method. Root-locus method and time-integration method [14] are used for the linear and non-linear aeroelastic analyses. LCO characteristics and the effects of asymmetric bilinear spring are investigated.

## 2. Theoretical analysis

### 2.1. Two-dimensional typical section model

Most tube-launched projectiles have deployable missile control fins like those shown in Fig. 1. These fins can be folded against the projectile body and allow more efficient use of space. Except

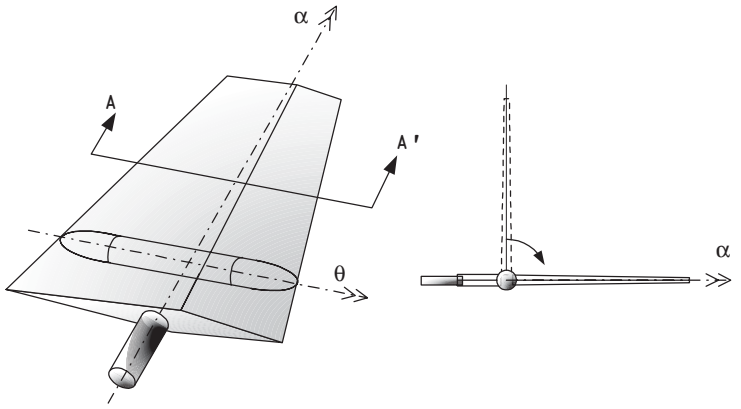


Fig. 1. Deployable missile control fin.

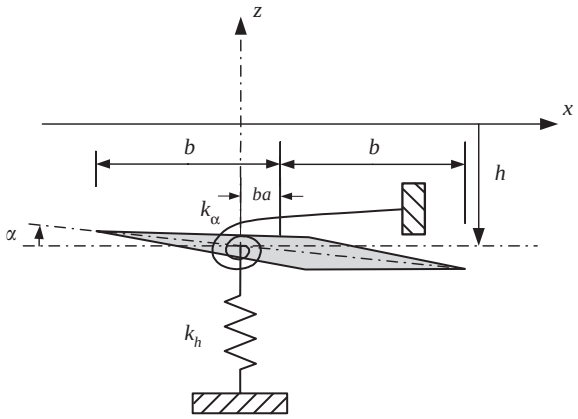


Fig. 2. Two-dimensional typical section model.

for the flexible modes of the fin, the cross-section AA′ has plunge and pitch rigid-body motions and is represented by the two-dimensional typical section model shown in Fig. 2. The two-dimensional model in Fig. 2 gives us a simple and easy method of aeroelastic analysis and provides easier understanding of physical meanings about aeroelastic characteristics. The present study considers the structural non-linearity in only a plunge spring.

### 2.2. Aeroelastic equation

The aeroelastic equations of the two-dimensional typical section model shown in Fig. 2 can be written as

$$\begin{bmatrix} m & S_\alpha \\ S_\alpha & I_\alpha \end{bmatrix} \begin{Bmatrix} \ddot{h} \\ \ddot{\alpha} \end{Bmatrix} + \begin{bmatrix} C_h & 0 \\ 0 & C_\alpha \end{bmatrix} \begin{Bmatrix} \dot{h} \\ \dot{\alpha} \end{Bmatrix} + \begin{bmatrix} K_h(h) & 0 \\ 0 & K_\alpha \end{bmatrix} \begin{Bmatrix} h \\ \alpha \end{Bmatrix} = \begin{Bmatrix} -L \\ M \end{Bmatrix}, \tag{1}$$

where $L$ and $M$ are the aerodynamic lift and moment, respectively.

If the motion is harmonic, the aerodynamic forces can be written as

$$\begin{Bmatrix} -L \\ M \end{Bmatrix} = q \begin{bmatrix} Q_{hh} & Q_{h\alpha} \\ Q_{\alpha h} & Q_{\alpha\alpha} \end{bmatrix} \begin{Bmatrix} h \\ \alpha \end{Bmatrix} = q[Q]\{x\}, \tag{2}$$

where $q\left(=\frac{1}{2}\rho U^2\right)$, $[Q]$, and $\{x\}$ are dynamic pressure, the aerodynamic influence coefficient (AIC) matrix, and the displacement vector, respectively.

The aeroelastic equations in Eq. (1) can be rewritten as

$$[M]\{\ddot{x}\} + [C]\{\dot{x}\} + [K]\{x\} = q[Q]\{x\} + \{f\}, \tag{3}$$

where

$$[M] = \begin{bmatrix} m & S_\alpha \\ S_\alpha & I_\alpha \end{bmatrix}, \quad [C] = \begin{bmatrix} C_h & 0 \\ 0 & C_\alpha \end{bmatrix}. \tag{4}$$

Stiffness matrix and the non-linear term in Eq. (3) are written as

$$[K] = \begin{bmatrix} K_h & 0 \\ 0 & K_\alpha \end{bmatrix}, \quad \{f\} = \begin{Bmatrix} 0 \\ 0 \end{Bmatrix} \tag{5}$$

for a linear system, and

$$[K] = \begin{bmatrix} 0 & 0 \\ 0 & K_\alpha \end{bmatrix}, \quad \{f\} = \begin{Bmatrix} -K_h(h)h \\ 0 \end{Bmatrix} \tag{6}$$

for a non-linear system.

### 2.3. State-space equation

To integrate the aeroelastic equations in Eq. (3), Eq. (3) may be transformed into state-space equations. In the present study, the AIC are calculated for several reduced frequencies $k$ by supersonic DPM code [14]. Thus, the aerodynamic coefficients should be approximated by a rational function. There are many methods for rational function approximation (RFA), and Karpel's minimum-state approximation (MSA) [13] is used here. The approximation form of Karpel's method is as follows:

$$[Q(s)] = [P_1]\left(\frac{b}{U}\right)^2 s^2 + [P_2]\left(\frac{b}{U}\right)s + [P_3] + [D](s[I] - [\bar{R}])^{-1}[E]s, \tag{7}$$

where $[P_i]$, $[D]$, and $[E]$ are calculated from a least-squares fit and $[R]$ is a diagonal matrix. The diagonal terms of $[R]$ are the aerodynamic poles and constants to be determined for best fit of $[Q]$.

Using Laplace transformation and MSA, Eq. (3) can be written as

$$([\bar{M}]s^2 + [\bar{C}]s + [\bar{K}])\{X(s)\} = [\bar{D}]\{X_a(s)\} + \{F(s)\}, \tag{8}$$

where

$$[\bar{M}] = [M] - \tfrac{1}{2}\rho b^2[P_1], \tag{9a}$$

$$[\bar{C}] = [C] - \tfrac{1}{2}\rho Ub[P_2], \tag{9b}$$

$$[\bar{K}] = [K] - \tfrac{1}{2}\rho U^2[P_3], \tag{9c}$$

$$[\bar{D}] = \tfrac{1}{2}\rho U^2[D]. \tag{9d}$$

In Eq. (8), the state vector $X_a(s)$ by the aerodynamic approximation is obtained as

$$\{X_a(s)\} = (s[I] - [\bar{R}])^{-1}[E]s\{X(s)\}. \tag{10}$$

Defining the new state $v$ as $\dot{x}$, the final state-space aeroelastic equations are obtained as

$$\begin{Bmatrix} \dot{v} \\ \dot{x} \\ \dot{x}_a \end{Bmatrix} = \begin{bmatrix} -[\bar{M}]^{-1}[\bar{C}] & -[\bar{M}]^{-1}[\bar{K}] & -[\bar{M}]^{-1}[\bar{D}] \\ [I] & [0] & [0] \\ [E] & [0] & [\bar{R}] \end{bmatrix} \begin{Bmatrix} v \\ x \\ x_a \end{Bmatrix} + \begin{Bmatrix} [\bar{M}]^{-1}\{f\} \\ 0 \\ 0 \end{Bmatrix}. \tag{11}$$

### 2.4. Method of aeroelastic analysis

The aeroelastic analysis is subdivided into a frequency-domain analysis and a time-domain analysis [15]. Frequency- and time-domain methods have differences in their approaches, but these methods give similar results for a linear aeroelastic problem.

The frequency-domain analysis has the advantages of relatively less computation time, simplicity of the analysis procedure, and ease of physical interpretation. However, this method cannot be directly applied to an aeroelastic problem with structural non-linearities. To overcome this disadvantage, these non-linearities should be linearized by a linearization method such as a describing function method. The advantage of time-domain analysis is that this method can be applied to both linear and non-linear problems, but the disadvantages are relatively more computation time, complexity of analysis procedure, and difficulty of physical interpretation. Therefore, an aeroelastic analysis with structural non-linearities should be performed by using both methods for an effective and accurate analysis [15].

In the present study, root-locus method and time integration method are used for non-linear aeroelastic analysis. The root-locus method involves tracing the root-loci of Eq. (11). As the air speed $U$ is increased, a real part eigenvalue of Eq. (11) is changed from negative to positive. This point is the flutter point. To integrate Eq. (11), the adaptive Runge–Kutta method [16] with step doubling and adaptive step-size control schemes is used here.

### 2.5. Asymmetric bilinear spring

Bae [14] established a non-linear hinge model of a deployable missile control fin from dynamic tests. In the present study, a plunge spring is represented by the asymmetric bilinear spring shown in Fig. 3. Relations between non-linear restoring force and displacement can be written as

$$f(x) = \begin{cases} K_1 x & \text{for } x < s_1, \\ (K_1 - K_2)s_1 + K_2 x & \text{for } s_1 < x < s_2, \\ (K_1 - K_2)s_1 + (K_2 - K_3)s_2 + K_3 x & \text{for } s_2 < x, \end{cases} \tag{12}$$

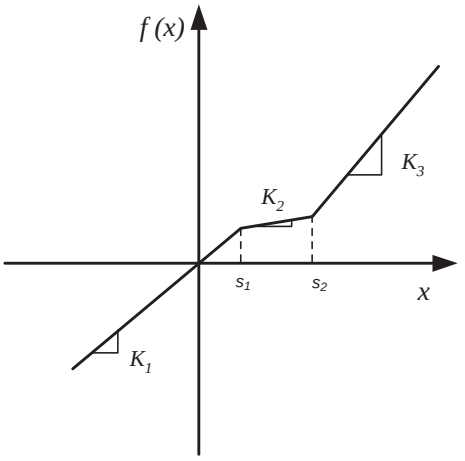


Fig. 3. General asymmetric bilinear spring.

where

$$K_2 = a_1 K_1, \quad K_3 = a_2 K_1. \tag{13}$$

For frequency-domain analysis, the equivalent stiffness of a non-linear spring in Eq. (12) should be obtained. The general describing function method [2] can give the method of an equivalent linear system but it cannot be used here. To account for general cases like the asymmetric bilinear spring shown in Fig. 3, a dual-input describing function technique [17] should be used. Considering a DC offset, an input $x$ is assumed as

$$x = B + A \sin \omega t. \tag{14}$$

Using the dual-input describing function and considering only the fundamental components, the restoring force is given as

$$f(t) = \bar{a}_0 + \bar{a}_1 \cos \omega t + \bar{b}_1 \sin \omega t, \tag{15}$$

where

$$\bar{a}_0 = \frac{1}{2\pi} \int_{-\pi}^{\pi} f \, \mathrm{d}(\omega t), \tag{16a}$$

$$\bar{a}_1 = \frac{1}{\pi} \int_{-\pi}^{\pi} f \cos(\omega t) \, \mathrm{d}(\omega t), \tag{16b}$$

$$\bar{b}_1 = \frac{1}{\pi} \int_{-\pi}^{\pi} f \sin(\omega t) \, \mathrm{d}(\omega t). \tag{16c}$$

Substituting Eq. (12) into Eqs. (15) and (16), coefficients $\bar{a}_0$, $\bar{a}_1$ and $\bar{b}_1$ can be obtained and simplified as follows:

(a)

$$A_1 (= A + B) \leqslant s_1,$$

$$f(t) = K_1 (A \sin \omega t + B),$$

$$\bar{a}_0 = K_1 B,$$

$$\bar{b}_1 = K_1 A,$$

(b)

$$s_1 < A_1 < s_2, \quad \gamma_1 = \sin^{-1}\left(\frac{s_1 - B}{A}\right),$$

$$f(t) = \begin{cases} K_1(A\sin\omega t + B), & -\pi \leqslant \omega t \leqslant \gamma_1, \ \ \pi - \gamma_1 \leqslant \omega t \leqslant \pi, \\ K_2(A\sin\omega t + B) + (K_1 - K_2)s_1, & \gamma_1 < \omega t < \pi - \gamma_1, \end{cases}$$

$$\bar{a}_0 = K_1 B + \frac{A}{\pi}(K_1 - K_2)\left(\frac{\pi - 2\gamma_1}{2}\sin\gamma_1 - \cos\gamma_1\right),$$

$$\bar{b}_1 = \frac{K_1 + K_2}{2}A + \frac{A}{2\pi}(K_1 - K_2)\,(2\gamma_1 + \sin 2\gamma_1),$$

(c)

$$s_2 \leqslant A_1, \quad \gamma_1 = \sin^{-1}\left(\frac{s_1 - B}{A}\right), \quad \gamma_2 = \sin^{-1}\left(\frac{s_2 - B}{A}\right)\gamma_2 = \sin^{-1}\left(\frac{s_2 - B}{A}\right),$$

$$f(t) = \begin{cases} K_1(A\sin\omega t + B), & -\pi \leqslant \omega t \leqslant \gamma_1, \\ & \pi - \gamma_1 < \omega t \leqslant \pi, \\ K_2(A\sin\omega t + B) + (K_1 - K_2)s_1, & \gamma_1 < \omega t \leq \gamma_2, \\ & \pi - \gamma_2 \leqslant \omega t \leqslant \pi - \gamma_1, \\ K_3(A\sin\omega t + B) + (K_2 - K_3)s_2 + (K_1 - K_2)s_1, & \gamma_2 < \omega t \leqslant \pi - \gamma_2, \end{cases}$$

$$\bar{a}_0 = K_1 B + \frac{A}{\pi}\left[(K_1 - K_2)\left(\frac{\pi - 2\gamma_1}{2}\sin\gamma_1 - \cos\gamma_1\right) + (K_2 - K_3)\left(\frac{\pi - 2\gamma_2}{2}\sin\gamma_2 - \cos\gamma_2\right)\right],$$

$$\bar{b}_1 = \frac{K_1 + K_2}{2}A + \frac{A}{2\pi}[(K_1 - K_2)(2\gamma_1 + \sin 2\gamma_1) + (K_2 - K_3)(2\gamma_2 + \sin 2\gamma_2)],$$

where $\bar{a}_1$ is zero for all cases. Because the describing functions depend on the amplitudes $A$ and $B$ of oscillation, an iterative approach is required [18].

Fig. 4 shows the variations of equivalent stiffness and amplitude $B$. Freeplay $\delta$ and amplitude $A_1$ are defined as

$$\delta = (s_2 - s_1)/2, \tag{13'}$$

$$A_1 = A + B, \tag{14'}$$

where the freeplay $\delta$ is designated as 0.1 mm. As the amplitude $A_1$ increases, the equivalent stiffness decreases within freeplay and increases outside of this value. Thus, an asymmetric

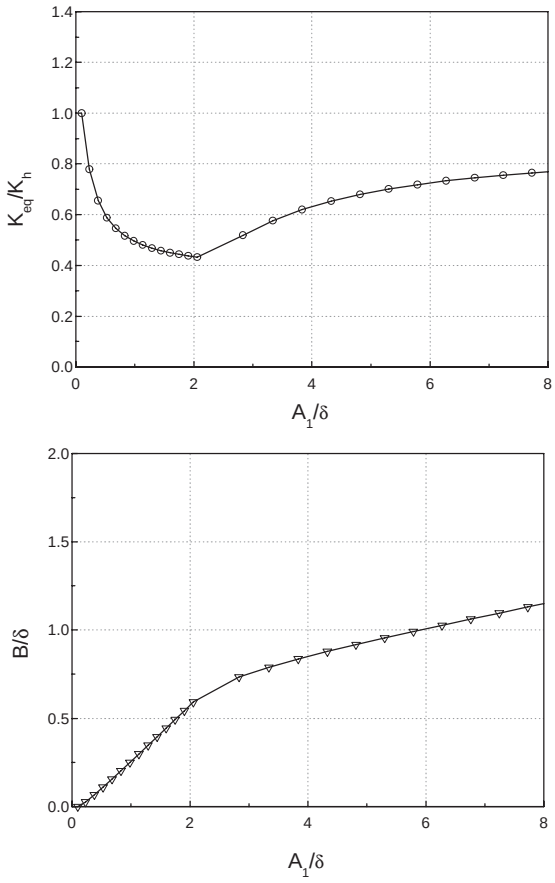


Fig. 4. Equivalent stiffness and $B$ for $a_1 = 0.2$, $a_2 = 0.8$ and $s_1/\delta = 0.1$.

bilinear spring has the characteristics of both softening and hardening springs for different amplitudes.

## 3. Numerical example and discussion

As a numerical example, the aeroelastic system parameters in Table 1 are used for linear and non-linear aeroelastic analyses. Mach number and air density used in the analyses are 2.0 and $1.25 \times 10^{-13}$ kgf s$^2$/mm$^4$, respectively. AIC matrix $[Q]$ in Eq. (2) is obtained by supersonic DPM. Generally, DPM gives the three-dimensional aerodynamic forces but the AIC of a typical section model can be obtained by considering a rectangular wing with a high aspect ratio.

### 3.1. Linear aeroelastic characteristics

Figs. 5 and 6 show the effects of plunge stiffness variations on the linear flutter characteristics for the frequency ratio of 0.765 and 1.3, respectively. The frequency ratio means the ratio of $\omega_h$ to

Table 1
System parameters of two-dimensional typical section model

| Parameter | Values |
|---|---|
| $b$ | 52.5 mm |
| $S_\alpha$ | $1.72 \times 10^{-4}$ kgf s$^2$ |
| $I_\alpha$ | $1.08 \times 10^{-2}$ kgf s$^2$/mm |
| $m$ | $2.04 \times 10^{-5}$ kgf s$^2$/mm |
| $\omega_h$ | 130 Hz |
| $e\ (= b(1+a))$ | 44.1 mm |

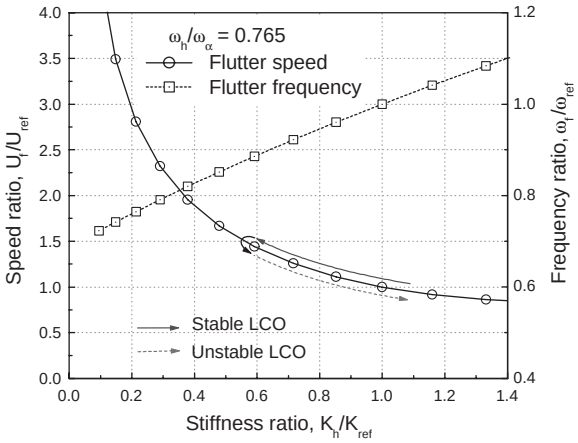


Fig. 5. Effects of $K_h$ on linear flutter characteristics ($\bar{\omega} = 0.765$).

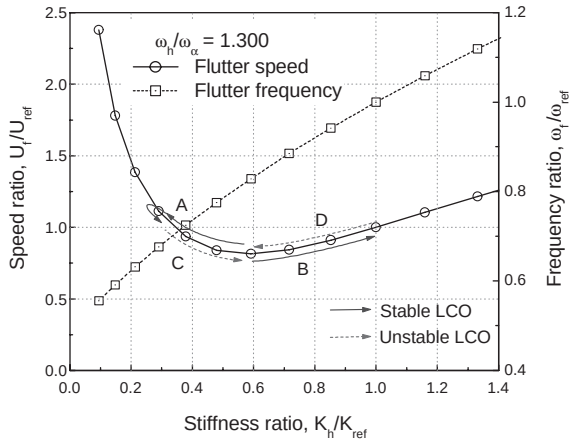


Fig. 6. Effects of $K_h$ on linear flutter characteristics ($\bar{\omega} = 1.3$).

$\omega_\alpha$. When the frequency ratio is 0.765, the flutter speed increases as the stiffness ratio decreases. The typical flutter of two-dimensional model is the plunge–pitch mode coalescence flutter. The decrease of plunge stiffness makes the plunge mode far from the pitch mode such that the flutter speed increases. When the frequency ratio is 1.3, the flutter speed decreases and then increases as the stiffness ratio decreases. This is caused by the exchange between plunge mode and pitch mode. As the stiffness ratio decreases, plunge mode coalesces with pitch mode, and then goes far from this mode. Thus, the linear aeroelastic characteristics of the two-dimensional model are significantly dependent on the frequency ratio. However, the flutter frequency is independent of the frequency ratio and decreases as the stiffness ratio decreases.

As shown in Fig. 3, the equivalent stiffness of an asymmetric bilinear spring decreases due to the structural non-linearity. Similar to the linear case, the non-linear aeroelastic characteristics are expected to be considerably dependent on the frequency ratio, as is discussed in the following section.

### 3.2. Non-linear aeroelastic characteristics

Fig. 7 shows the LCO flutter characteristics of the two-dimensional model with an asymmetric bilinear plunge spring when the frequency ratio is 0.765. As shown in Fig. 7, the results of frequency-domain analyses using describing function and time-domain analysis agree well with each other. For the frequency ratio of 0.765, LCOs are observed above the linear flutter speed because the flutter speed increases due to the decrease of the equivalent stiffness as shown in Fig. 5. The LCOs in Fig. 7 are of two different types. One is a stable LCO 'A' with a small amplitude and the other is an unstable LCO 'B' with a large amplitude. The two different types of LCOs are dependent on an initial condition, and unstable LCO is observed at the boundary between stable LCO and divergent flutter. Fig. 8 shows the aeroelastic responses with the two different LCOs when the speed ratio ($U^* = U/U_{ref}$) is 1.4. A large-amplitude LCO disappears and then a small-amplitude LCO remains. An unstable LCO transiently occurs when the initial amplitude ratio ($h_0^* = h_0/\delta$) is about 2.66. When the initial condition is less than that value, only the small-amplitude LCO occurs, and when the initial condition is greater, the aeroelastic response becomes

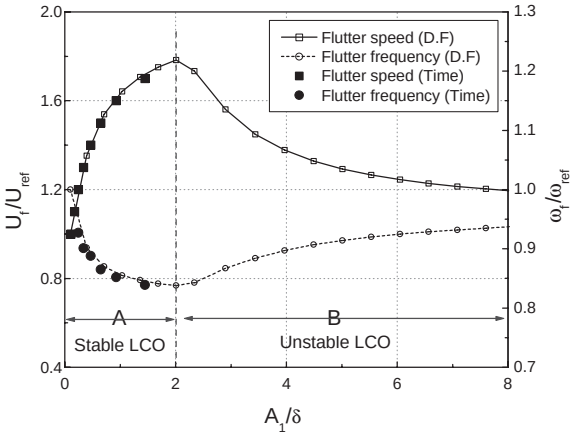


Fig. 7. LCO flutter characteristics with asymmetric bilinear spring ($\bar{\omega} = 0.765$).

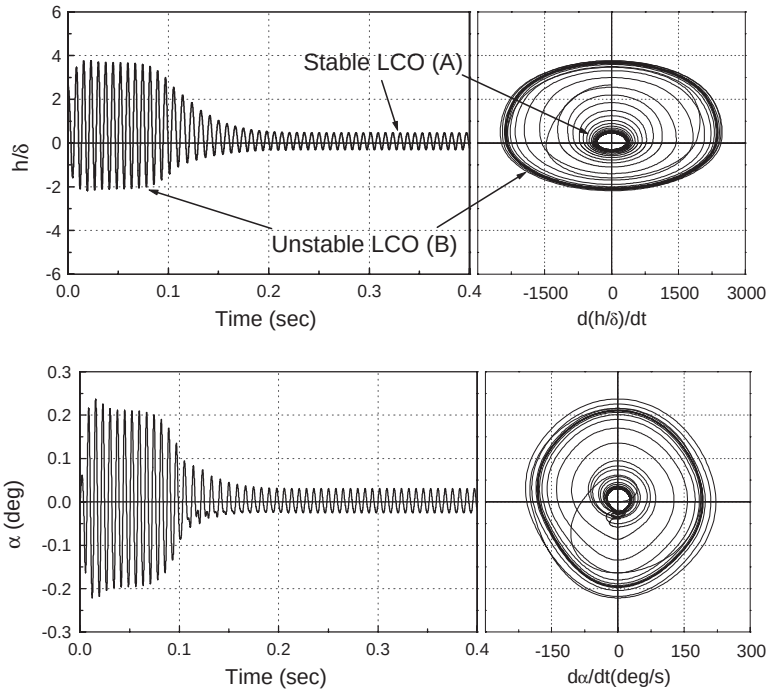


Fig. 8. Two types of LCO for $\bar{\omega} = 0.765$, $U^* = 1.4$, and $h_0^* = 2.66$.

unstable. Thus, the large-amplitude LCO can make the aeroelastic system unstable and this is dependent on the initial condition. Beyond the flutter velocity, the amplitude of the stable LCO increases as the flow velocity increases, while the amplitude of the unstable LCO decreases. At a flow velocity of about 1.8, the amplitudes of the stable and unstable LCO merge. Beyond that flow velocity, no stable LCO is possible and the system will only experience a diverging oscillation. This can be explained by Fig. 5. As shown in Fig. 4, the characteristics of an asymmetric bilinear spring change from a softening spring to a hardening spring as the amplitude ratio increases. As the arrows indicate in Fig. 5, the flutter speed increases due to the decrease of stiffness and then the flutter speed decreases due to the increase of stiffness. A stable LCO occurs in the speed-increased path (straight line) and an unstable LCO occurs in the speed-decreased path (dashed line).

Fig. 9 shows the parameter map of the two-dimensional model with an asymmetric bilinear spring when the frequency ratio is 0.765. The parameter map shows the types of aeroelastic responses for various speed ratios and initial amplitude ratios. When the speed ratio is greater than 1.0, LCOs are observed. At the same speed, LCOs or divergent aeroelastic responses are observed dependent on an initial amplitude ratio. Complicated motion such as LCO with two or more periods and chaotic motion is not observed.

Fig. 10 shows the LCO flutter characteristics of the two-dimensional model with an asymmetric bilinear plunge spring when the frequency ratio is 1.3. The results of frequency-domain analysis and time-domain analysis agree well with each other. When the frequency ratio is 1.3, four

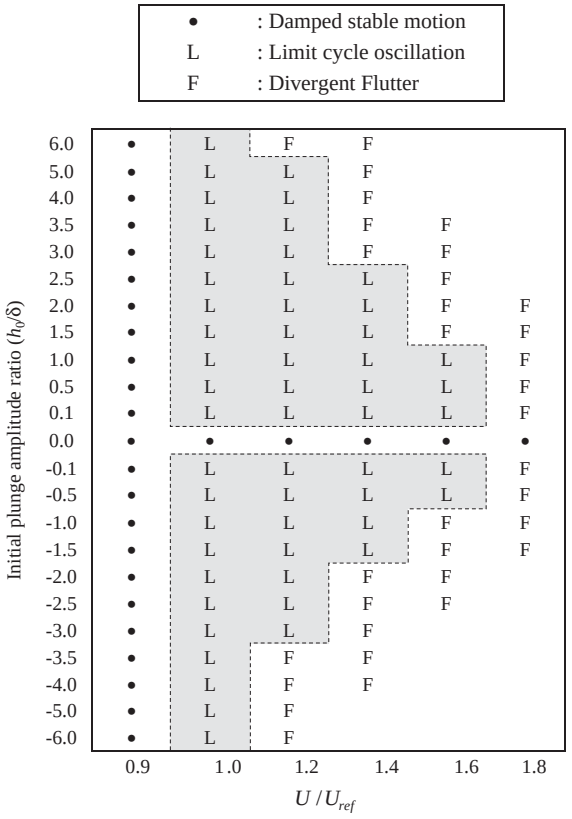


Fig. 9. Parameter map of two-dimensional model with asymmetric bilinear spring ($\bar{\omega} = 0.765$).

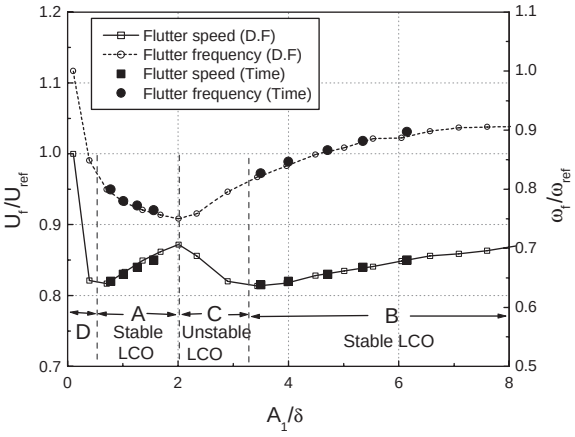


Fig. 10. LCO flutter characteristics with asymmetric bilinear spring ($\bar{\omega} = 1.3$).

different types of LCO are observed below the linear flutter speed as shown in Fig. 10. Two LCOs are stable LCOs, 'A' and 'B' in Fig. 10, and two are unstable LCOs, 'C' and 'D'. These different LCOs are dependent on the initial condition. Although the authors could not observe unstable

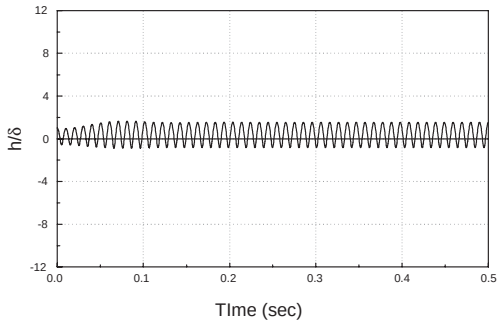


(a) Stable LCO A($h_0^* = 1.0$)

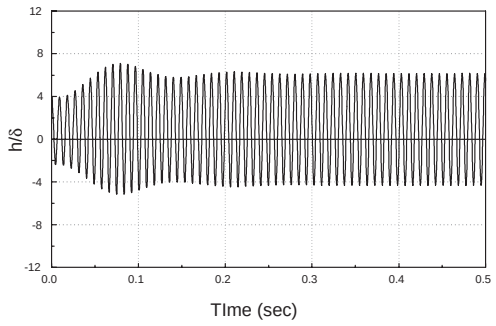


(b) Stable LCO B($h_0^* = 4.0$)

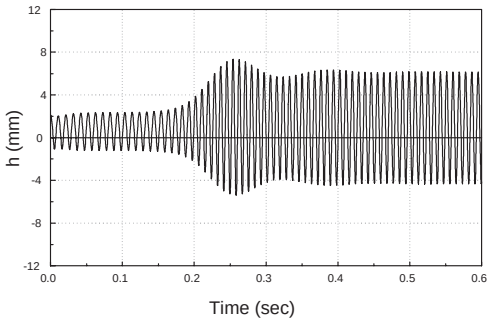


(c) Unstable LCO C & Stable LCO B($h_0^* = 2.1$)

Fig. 11. Three types of LCO for $\bar{\omega} = 1.3$ and $U^* = 0.85$.

LCO 'D' in the time-domain analysis, one might infer its presence if the initial condition is sufficiently small. Fig. 11 shows the three types of LCOs when the speed ratio is 0.85. Figs. 11(a) and (b) show the stable small-amplitude LCO 'A' and stable large-amplitude LCO 'B', respectively. Fig. 11(c) shows that the unstable LCO 'C' disappears and stable LCO 'B' remains. As the amplitude ratio increases, LCO characteristics follow the path of D–A–C–B, as the arrows indicate in Fig. 6. Stable LCOs are observed in the two speed-increased paths and unstable LCOs are observed in the two speed-decreased paths. Thus, the LCOs in Fig. 10 have double LCO characteristics that consist of A–C LCO, as in Fig. 7, and D–B LCO. Fig. 12 shows the double LCO. Two different LCOs X and Y are combined into the complicated LCO shown in Fig. 10 such that it represents the characteristics of the two stable LCOs and two unstable LCOs.

Fig. 13 shows the parameter map when the frequency ratio is 1.3. When the speed ratio is between about 0.8 and 1.0, LCOs are observed. At the same speed ratio, different types of LCOs are observed dependent on initial conditions. However, aeroelastic responses do not become unstable due to initial conditions. When the initial amplitude ratio is less than $\pm 0.1$, LCOs are not observed. When the speed ratio is greater than about 0.9, LCOs are observed, but this region can be defined as a divergent flutter because the LCO amplitude is so large. Complicated motions are not observed.

Figs. 14–17 show the time histories and phase plots of the two-dimensional model when the speed ratio is 0.82. Fig. 14 shows a stable small-amplitude LCO 'A' when the initial amplitude

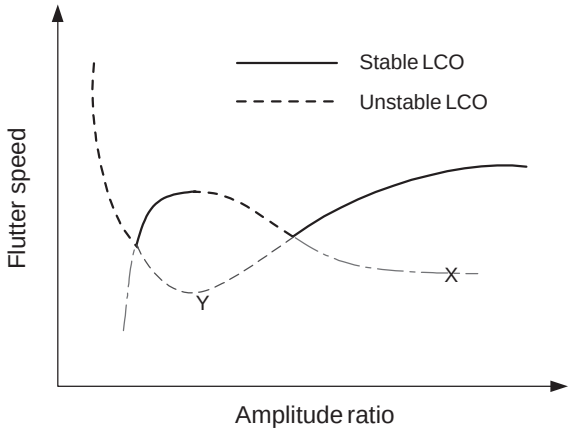


Fig. 12. Double limit cycle oscillation.

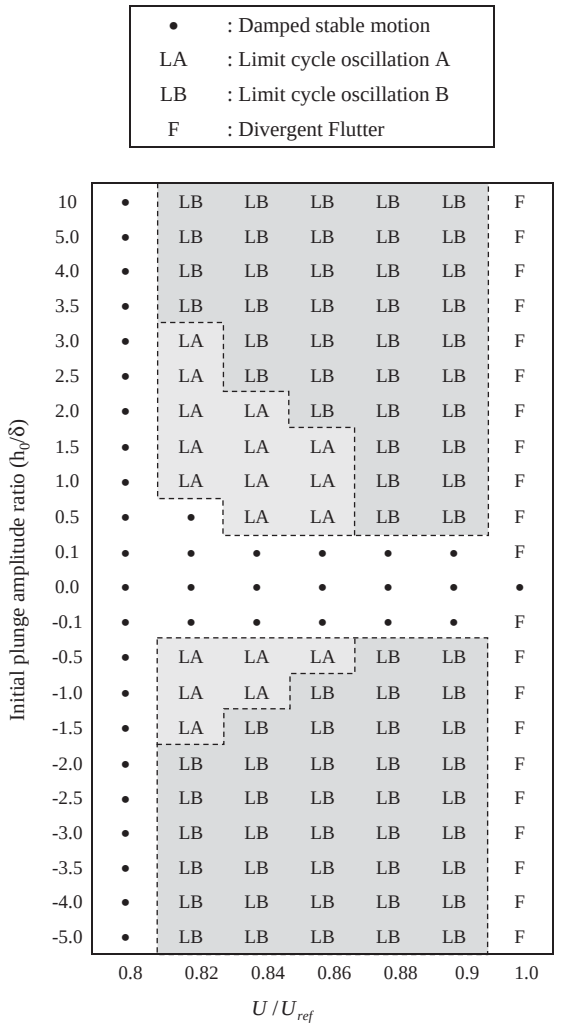


Fig. 13. Parameter map of two-dimensional model with asymmetric bilinear spring ($\bar{\omega} = 1.3$).

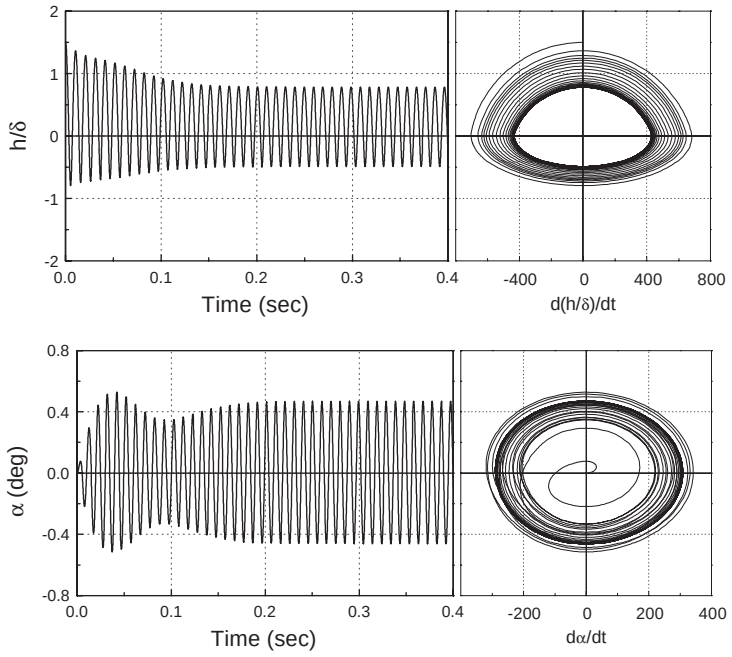


Fig. 14. Time history and phase plot of two-dimensional model ($U^* = 0.82$, $h_0^* = 1.5$).

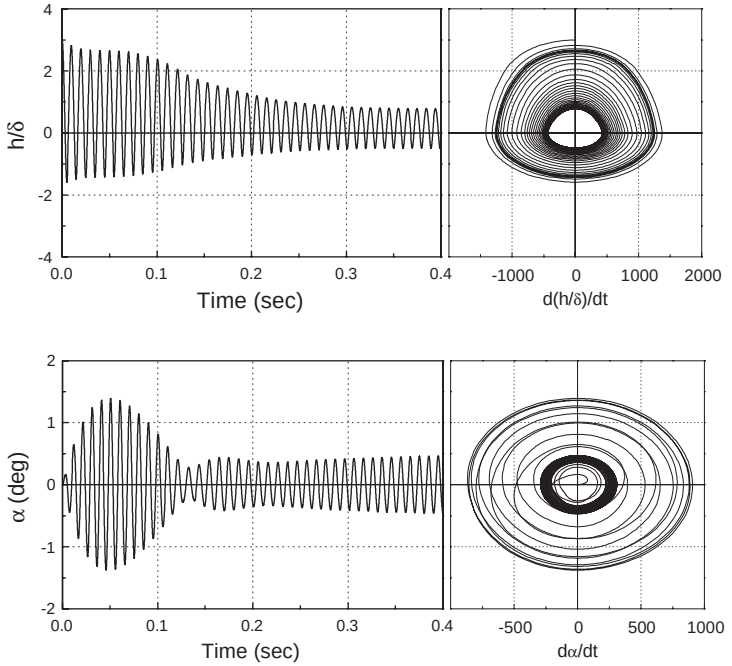


Fig. 15. Time history and phase plot of two-dimensional model ($U^* = 0.82$, $h_0^* = 3.0$).

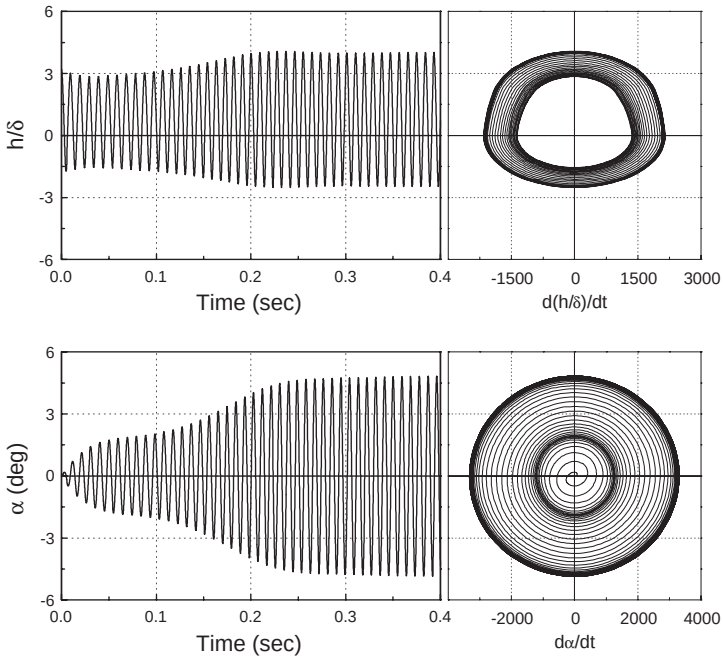


Fig. 16. Time history and phase plot of two-dimensional model ($U^* = 0.82$, $h_0^* = 3.2$).

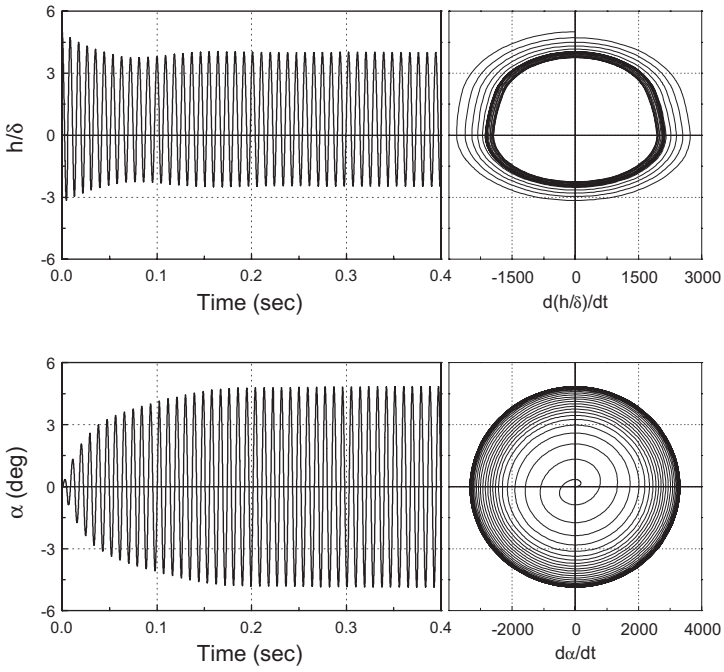


Fig. 17. Time history and phase plot of two-dimensional model ($U^* = 0.82$, $h_0^* = 5.0$).

ratio $h_0^*$ is 1.5. When $h_0^*$ is 3.0, the unstable LCO 'C' transiently disappears and stable small-amplitude LCO remains, as shown in Fig. 15. Fig. 16 shows that the unstable LCO 'C' becomes a stable large-amplitude LCO 'B' when $h_0^*$ is 3.2. Fig. 17 shows that only stable large-amplitude LCO 'B' is observed when $h_0^*$ is 5.0. Unstable LCO could make the system unstable when the frequency ratio is 0.765, whereas unstable LCO does not make the system unstable when the frequency is 1.3. Unstable LCO 'C' disappears due to the stable LCO 'B' and the system remains stable.

## 4. Conclusions

To investigate the non-linear aeroelastic characteristics of a deployable missile control fin, non-linear aeroelastic analyses of a two-dimensional typical section with an asymmetric bilinear plunge spring are performed in the frequency domain and the time domain. DPM is used for the calculation of supersonic aerodynamic forces and MSA is used for the aerodynamic approximation. An asymmetric bilinear spring is linearized using the dual-input describing function method. Root-locus method and time-integration method are used for linear and non-linear aeroelastic analyses.

An asymmetric bilinear spring has the characteristics of both softening and hardening springs for the variations of LCO amplitude and it considerably affects the linear and non-linear aeroelastic characteristics. From aeroelastic analyses, LCOs can be observed below or above the flutter speed. LCO characteristics of the aeroelastic system are significantly dependent on the frequency ratio. When the frequency ratio is less than 1.0, stable small-amplitude LCO and unstable large-amplitude LCO are observed above the flutter speed. When the frequency ratio is greater than 1.0, double LCO, which consists of two stable LCOs and two unstable LCOs, is observed below the flutter speed and the non-linear flutter boundary is then lower than the linear flutter boundary. Thus, the frequency ratio plays an important role in the non-linear aeroelastic characteristics of an aeroelastic system.

## Acknowledgements

This research was supported by Agency for Defense Development (ADD) and the Ministry of Science and Technology (National Research Laboratory Program) in the Republic of Korea. This support is gratefully acknowledged.

## Appendix A. Nomenclature

| | |
|---|---|
| $b$ | reference length, half-chord |
| $B$ | DC amplitude |
| $[C]$ | damping matrix |
| $f$ | non-linear term |
| $F(s)$ | Laplace transforms of $f$ |

| | |
|---|---|
| $h$ | plunge displacement |
| $h_0^*$ | initial amplitude ratio |
| $I_\alpha$ | moment of inertia |
| $K_h$ | linear plunge stiffness |
| $K_h(h)$ | non-linear plunge stiffness |
| $K_\alpha$ | pitch stiffness |
| $[K]$ | stiffness matrix |
| $m$ | mass of wing |
| $[M]$ | mass matrix |
| $q$ | dynamic pressure |
| $s$ | Laplace variable |
| $S_\alpha$ | mass unbalance |
| $[Q]$ | aerodynamic influence coefficient matrix |
| $U$ | air speed |
| $U_{ref}$ | linear flutter speed |
| $x$ | displacement vector |
| $x_a$ | augmented state by aerodynamic approximation |
| $X(s)$ | Laplace transforms of $x$ |
| $X_a(s)$ | Laplace transforms of $x_a$ |
| $\alpha$ | pitch angle |
| $\delta$ | freeplay |
| $\rho$ | air density |
| $\omega_\alpha$ | pitch frequency |
| $\omega_h$ | plunge frequency |

*Subscripts*

| | |
|---|---|
| $h$ | plunge |
| $\alpha$ | pitch |

## References

[1] D.S. Woolston, H.W. Runyan, R.E. Andrews, An investigation of effects of certain type of structural nonlinearities on wing and control surface flutter, Journal of Aeronautical Sciences 24 (1957) 57–63.
[2] R.M. Laurenson, R.M. Trn, Flutter analysis of missile control surface containing structural nonlinearities, AIAA Journal 18 (1980) 1245–1251.
[3] C.L. Lee, An iterative procedure for nonlinear flutter analysis, AIAA Journal 24 (1986) 833–840.
[4] B.H.K. Lee, A. Tron, Effects of structural nonlinearities on flutter characteristics of the CF-18 aircraft, Journal of Aircraft 26 (1989) 781–786.
[5] Z.C. Yang, L.C. Zhao, Analysis of limit cycle flutter of an airfoil in incompressible flow, Journal of Sound and Vibration 123 (1988) 1–13.
[6] I. Lee, S.H. Kim, Aeroelastic analysis of a flexile control surface with structural nonlinearity, Journal of Aircraft 32 (1995) 868–874.
[7] M.D. Conner, D.M. Tang, E.H. Dowell, L.N. Virgin, Nonlinear behavior of a typical airfoil section with control surface freeplay: a numerical and experimental study, Journal of Fluid and Structures 11 (1997) 89–109.

[8] D.M. Tang, E.H. Dowell, L.N. Virgin, Limit cycle behavior of an airfoil with a control surface, Journal of Fluids and Structures 12 (1999) 839–858.
[9] L. Virgin, M.D. Conner, E.H. Dowell, In the evolution of deterministic non-periodic behavior an airfoil, International Journal of Nonlinear Mechanics 34 (1999) 499–514.
[10] D.M. Tang, D. Kholodar, E.H. Dowell, Nonlinear response of airfoil section with control surface freeplay to gust loads, AIAA Journal 38 (2000) 1543–1557.
[11] E.F. Sheta, V.J. Harrand, D.E. Thomson, T.W. Strganac, Computational and experimental investigation of limit cycle oscillations of nonlinear aeroelastic systems, Journal of Aircraft 39 (2002) 133–141.
[12] T. Ueda, E.H. Dowell, Doublet point method for supersonic unsteady lifting surfaces, AIAA Journal 22 (1984) 179–186.
[13] M. Karpel, Design for active flutter suppression and gust alleviation using state-space aeroelastic modeling, Journal of Aircraft 19 (1982) 221–227.
[14] J.S. Bae, Aeroelastic Characteristics and Flutter Suppression Considering Structural Nonlinearity, Ph.D. Dissertation, Department of Aerospace Engineering, Korea Advanced Institute of Science Technology, 2002.
[15] J.S. Bae, S.M. Yang, I. Lee, Linear and nonlinear aeroelastic analysis of a fighter-type wing with control surface, Journal of Aircraft 39 (2002) 697–708.
[16] W.H. Press, B.P. Flanner, S.A. Teukolsky, W.T. Vetterling, Numerical Recipes: The Art of Scientific Computation, Cambridge University Press, Cambridge, 1986.
[17] A. Gelb, W.E. Vander Velde, Multiple-Input Describing Functions and Nonlinear System Design, McGraw-Hill, New York, 1986.
[18] S.J. Price, H. Alighanbari, B.H.K. Lee, AIAA-94-1546-CP. The Aeroelastic Response of a Two-dimensional Airfoil with Bilinear and Cubic Structural Nonlinearities, 1994.